A damage criterion based on energy balance for isotropic cohesive zone model

André Chrysochoos, Loïc Daridon, Mathieu Renouf

A damage criterion based on energy balance for isotropic cohesive zone model

André Chrysochoos[1,2], Loic Daridon[1,2], and Mathieu Renouf[1,2]

[1] LMGC, Université de Montpellier, CNRS, Montpellier, France
[2] MIST, Université de Montpellier, IRSN, CNRS, France

The objective of this paper is to present an energy damage criterion for cohesive zone models (CZM) within the framework of the non-linear thermodynamics of irreversible processes (TIP). An isotropic elastic damageable material is considered for isothermal transformations. Damage is then the only irreversible effect accompanying the deformation process and this mechanism is supposed to be fully dissipative. Once a separation law and a damage state variable have been chosen, the paper shows that the damage evolution law can be automatically derived from the energy balance. From this observation, a CZM is derived for a given choice of traction-separation law and damage state variable and the quality of its numerical predictions is analyzed using an experimental benchmark bending test extracted from literature. Damage, elastic and dissipated energy fields around the crack path are shown during this rupture test. Finally, a numerical simulation of a Brazilian test is proposed where no pre-crack is present in the specimen. Then, as before, the evolution of the dissipated energy fields are plotted during the loading until the total failure of the specimen.

Keywords cohesive zone, damage, fracture, thermodynamics of irreversible processes, energy balance, Finite element analysis,Brazilian test

1 Introduction

In many engineering applications, the fracture behavior of the structure is crucial, which is why damage mechanisms have been studied over the last decades, from a theoretical, numerical and experimental point of view, using different frameworks Amor et al. 2009; Lemaitre 1996. Since the pioneering work of L. M. Kachanov Kachanov 1986, continuum damage mechanics has become a scientific discipline focusing on the effects of various microdefects on the macroscopic behavior of materials and structures. Volume damage descriptions often use a damage variable linked to loss of stiffness Chaboche et al. 2001; Kondo et al. 2007. For a given elastic material, the stiffness tensor $\mathbf{E_d}$ at a certain level of isotropic damage, denoted by d, is very often related to the stiffness tensor $\mathbf{E_0}$ of the undamaged material as follows: $\mathbf{E_d} = (1-d)\mathbf{E_0}$. Thermodynamically speaking the elastic free energy of damageable material, ψ, is also defined in the same way $\psi = (1-d)\psi_0$, where ψ_0 is the elastic free energy of the non damaged material. The conjugate variable associated with the damage state variable, d, is by definition $Y_d = \frac{\partial \psi}{\partial d}$, leading to a thermodynamic force X_d which is given by $X_d = -Y_d = \psi_0$. Classically, for material behavior using threshold criterion, the thermodynamic force X_d is then used to define the damage rate $\dot{d}$, through a yield function F and its associated flow rule Lemaitre 1996.

An alternative numerical strategy to predict the evolution of damage and crack propagation is to introduce a 3D cohesive zone model (CZM) between two elastic layers. The CZM model is considered as a zero-thickness medium where the traction-separation law can be derived from a surface free energy. This numerical approach has been widely used in many areas of computational mechanics Allix et al. 1995; Suo et al. 1990; Needleman 1990; Daridon et al. 2011. To model elastic damageable materials, the main assumption is that all the damage that occurs in the bulk is gathered in a cohesive zone. In a finite element approach the cohesive zone is then located between two elements where elastic behavior remains linear Blal et al. 2011. Since the pioneering works carried out by Dugdale and Barenblatt Dugdale 1960, many cohesive-zone models were proposed in the literature Alfano et al. 2006; Corigliano et al. 2001; Chen et al. 2009. Cohesive-zone models taking fatigue into account were also developed to simulate crack propagation under cyclic loading conditions Roth et al. 2014; Nguyen et al. 2001 while others were developed to combine two irreversible phenomena such as damage and plasticity Kolluri et al. 2014. From an experimental standpoint, the identification of CZM requires the coupling of experimental data and numerical studies to accurately define the traction separation law Huon, V. et al. 2010; Chrysochoos et al. 2014; Richefeu et al. 2012.

A classic criticism of the cohesive zone methods is their relative dependency on mesh size. For example, intrinsic CZM approach for crack propagation has a deficiency of introducing artificial compliance to the model and crack path dependency because the cohesive elements are inserted between every 2D or 3D elements Zhou et al. 2004. To remedy this mesh dependency, associated with the vanishing of stiffness, a new class of so-called "non-local methods" has appeared in the domains of damage and fracture mechanics. Two main regularization techniques exist to avoid pathological localization, namely the integral Pijaudier-Cabot et al. 1987 or the gradient Lorentz et al. 1999; Amor et al. 2009 damage approaches. Both consist in introducing non-local terms in the formulae of the cohesive model associated with a characteristic length. For example, in the Thick Level Set method, which is an integral damage approach, the undamaged zone is separated from the totally damaged zone by a level set Moës et al. 2011. The damage variable is then an explicit function of the level set. The damage growth in solids is based on the movement of a layer of finite thickness l_c within which the damage varies continuously. Then, the damage rate is directly linked to the set propagation. The non-local aspect of this method is essentially due to the fact that the configurational force driving the damage front is an average value over the thickness of the level set in the wake of the front Lé et al. 2018; Bernard et al. 2012. As in bulk damage mechanics, this approach allows the cracks' initiation and propagation within the same framework.

Another way to regularize the damage progress is to add a gradient-dependent term and to derive the problem of damage evolution from a variational approach based on an energy formulation Marigo et al. 2016. This approach has also been used to couple the models for gradient-damage and those for plasticity Alessi et al. 2015 or to develop a cohesive zone model suitable for fatigue fracture Cazes et al.

2015; Abdelmoula et al. 2009; Pham et al. 2012. The macroscopic behavior can be seen as brittle fracture with a Griffith-like criterion associated with cohesive fracture of the Barenblatt or Dugdale types Daridon et al. 1997. The variational formulation of fracture mechanics framework has also been used to develop the Eigen-erosion scheme Pandolfi et al. 2013. In this finite element approximation scheme, the crack tracking problem is done by successively eroding elements when the attendant elastic energy releaseable exceeds the critical fracture energy.

The objective of the following sections is to construct an energy damage criterion for an isotropic elastic damageable material within the TIP framework. The damage law is based on the premise that the damage progress is linked to a prescribed evolution in the maximum elastic energy that can be stored within the material for a given damage state. The damage mechanisms are the only microstructural irreversible effects accompanying the deformation processes and these mechanisms are fully dissipative (no energy storage is induced by the material degradation). Naturally, damage dissipation may induce self heating leading to non-isothermal deformation processes that are consequently irreversible due to heat diffusion. However for sake of simplicity, only isothermal transformations are considered and the chosen state variables are the displacement jump $\mathbf{u}$ and a scalar damage variable, denoted by u_d. The damage variable u_d can be related to the effective displacement as used in Daridon et al. 2011; Park et al. 2009; Bosch et al. 2006; Blal et al. 2011.

The layout of the paper is as follows. The energy criterion of the damageable elastic cohesive zone model is presented in Section 2 through a 1D scenario within the TIP framework. In Section 3, a vectorial extension of the cohesive zone law is proposed for an isotropic damage evolution. In Section 4, the capability of the model is investigated using an experimental benchmark test (i.e. a single-edge notch-bending specimen for fracture toughness testing) Moës et al. 2011; Wojtacki et al. 2015; Galvez et al. 1996. Mechanical and energy responses are shown and discussed. In particular, several damage, elastic and dissipated energy fields around the fracture paths are plotted during the crack propagation. The computation of the dissipated energy fields is of special interest inasmuch as they can be compared with the ones derived from quantitative IR techniques. Indeed, it is possible to use infrared data to derive heat sources fields. Corresponding image processing techniques can be found in Chrysochoos 2012; Benaarbia et al. 2017. In this perspective, a numerical simulation of a Brazilian disc test is finally proposed. This kind of test is well adapted to infrared imaging inasmuch as the flat surface of the specimen remains perpendicular to the optical axis of the camera until the crack occurs.

2 1D scenario

The objective of the following section is to briefly review the mechanical concepts classically introduced with CZM in the case of a 1D monotonic traction and to embed them into the TIP framework to derive, through an energy criterion, a damage evolution law.

2.1 Mechanical aspects

In the literature, the mechanical response of the cohesive zone is described by the correspondence between the " normal traction" force f supported by the interface and its normal opening displacement often called "separation" during a monotonic opening. Depending on the chosen form of the traction-separation diagram, the relationships are called bilinear, polynomial or exponential cohesive laws. In Figure 1 a polynomial form has been chosen to illustrate the most commonly characteristics of these curves. We find the cohesive strength f_0 corresponding to the maximum of the traction–separation curve or its associated opening displacement u_0, the maximum value of separation u_c corresponding to the crack opening. An energy parameter is also often mentioned Ortiz et al. 1999: this is the fracture energy $A_c = \int_0^{u_c} f(u)du$ (work of separation), which is the area below the traction-separation curve.

This traction-separation curve is considered as a threshold over which the damage develops irreversibly. This threshold is an intrinsic characteristic of the cohesive zone behavior. When unloading is considered, it is supposed to be purely elastic, assuming that the damage progress stops as soon as the loading point is below the threshold curve. For convenience, the elastic unloading paths are often directed towards the origin of the traction–separation diagram (see Figure 1). This implies that the elasticity remains linear and that there is no residual opening at the end of the unloading.

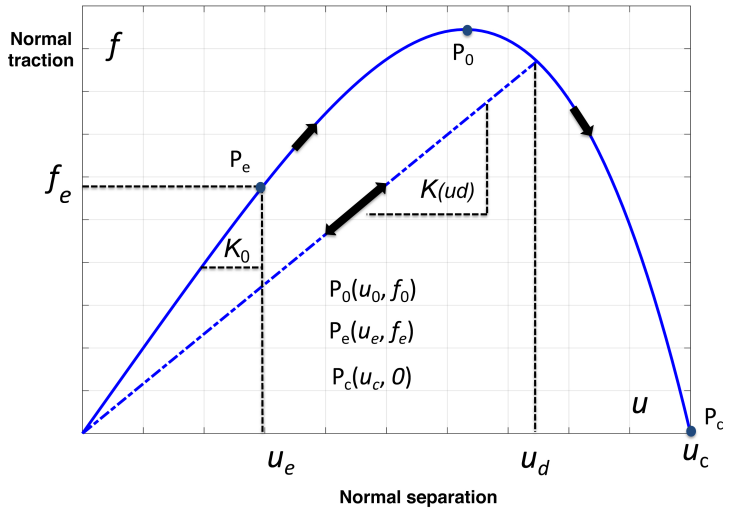

Figure 1: Traction-separation diagram. Monotonic envelope (continuous line), elastic unload or reload (dashed line). An arbitrary polynomial cohesive law has been chosen.

The progress of the damage can be depicted by a continuous decrease of the secant stiffness $K = \frac{f}{u}$ towards zero until rupture at u_c . A classical scalar definition of the damage variable can then be given by:

$$D_k = \frac{K_0 - K}{K_0}, \tag{1}$$

where K_0 is the initial stiffness of the cohesive zone. The variable D_k progressively increases from 0 to 1 when the opening displacement increases from 0 to u_c (or from u_e to u_c when a pure elastic domain,

$[0, u_e]$, is introduced in the traction-separation curve (see Figure 1)).

A second possibility is to consider a normalized deformation energy definition of the damage Ortiz et al. 1999 :

$$D_A = \frac{A}{A_c}, \text{ where } A = \int_0^u f(v)dv \, . \tag{2}$$

Here again, this last definition slightly changes when an elastic domain limited by the point (u_e, f_e) is introduced. In such a case, *Eq.*(2) requires a renormalization:

$$D_A^* = \frac{A^*}{A_c^*}, \text{ where } A^* = \int_{u_e}^u f(v)dv \text{ and } A_c^* = \int_{u_e}^{u_c} f(v)dv \, . \tag{3}$$

Then by construction D_A and D_A^* belong to $[0, 1]$. In fact, there are many ways to define damage. The damage process being assumed irreversible, the damage variable rate is often chosen to be non-negative whatever the loading history, to depict its monotonic evolution. Damage develops when the mechanical state (u, f) corresponds to a point of the cohesive threshold curve. In what follows we have chosen a kinematic definition of the damage variable. Like previously done by numerous authors (*e.g.* Serpieri et al. 2015), we have chosen the maximum value of the separation u_d ever reached by the cohesive zone until instant t. This damage variable is then defined at instant t by:

$$u_d = \max \{u(\tau), \forall \tau \leqq t\} \, . \tag{4}$$

This variable monotonically increases during the damage progress from 0 to u_c whatever the loading path (see Fig.1)) .

2.2 Energy aspects

Usually during a load cycle, the deformation energy w_{def}, which corresponds to the area surrounded by the loading curve *Eq.*(7) is transformed into dissipated energy, denoted by w_d, and stored energy, denoted by w_s, due to the irreversible microstructural transformations accompanying the deformation process. Part of w_{def} can also involve strong thermomechanical coupling energy (heat) w_{thm} Chrysochoos 2012. An illustrative example of the coupling effects on the mechanical response can be given by the famous thermoelastic damping presented by Zener in Zener 1938. The general form of the energy balance over a loading cycle can then be written as:

$$w_{def} = w_d + w_s + w_{thm} \, . \tag{5}$$

For any other loading the elastic energy, w_e, has to be added so that :

$$w_{def} = w_e + w_d + w_s + w_{thm} \, , \tag{6}$$

w_e vanishing, by construction, over a loading cycle. In the present situation, we only consider isothermal transformations with no thermomechanical coupling. Moreover, we assume that damage is a pure dissipative mechanism and that, consequently, no energy storage or release of stored energy, due to microstructural changes, occurs during the loading. These assumptions imply $w_s = 0$ and $w_{thm} = 0$. For any kind of separation-controlled loading $\{u(\tau), \forall \tau \leqq t\}$, the deformation energy at instant t is here defined by:

$$w_{def}(t) = \int_0^t f(\tau)\dot{u}(\tau)d\tau \, . \tag{7}$$

For monotonic loadings, the mechanical state follows the traction-separation curve. The deformation energy then represents the mechanical energy required to reach the damage state $u_d = u(t)$. This cost in deformation energy can be defined by:

$$w_{def}^d(u_d) = \int_0^{u_d} f(v)dv \, . \tag{8}$$

Another important mechanical energy term is the elastic energy, $w_e(u, u_d)$, in the cohesive zone at a given state of damage u_d. It is defined by:

$$w_e(u, u_d) = \frac{1}{2}K(u_d)u^2 \, . \tag{9}$$

Note that this energy is mechanically recoverable during the unloading. This is the reason why it did not appear in the general form of the energy balance proposed in *Eq.*(5) for a complete loading cycle.

As previously done for the deformation energy during monotonic loading, we can define the elastic energy $w_e^d(u_d)$ by:

$$w_e^d(u_d) = \frac{1}{2}K(u_d)u_d^2 = w_e(u_d, u_d) \, , \tag{10}$$

which represents the maximum elastic energy mechanically recoverable for a given damage state, defined by u_d.

As previously supposed (no thermomechanical coupling energy, no energy storage) the difference

between $w^d_{def}(u_d)$ and $w^d_e(u_d)$ is attributed to the energy dissipation accompanying the irreversibility of damage mechanisms. The dissipated energy, $w^d_d(u_d)$, is then defined by :

$$w^d_d(u_d) = w^d_{def}(u_d) \; - \; w^d_e(u_d) \; , \tag{11}$$

$w^d_d(u_d)$, $w^d_e(u_d)$ and $w^d_{def}(u_d)$ are illustrated in Figure 2.

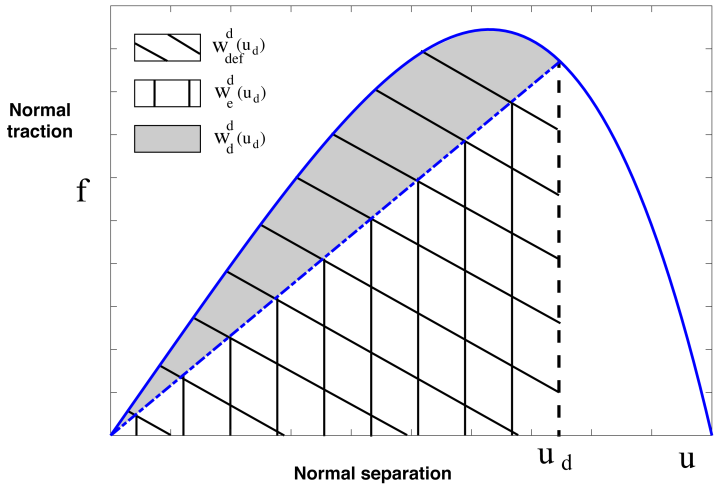

Figure 2: Energy illustration of the traction-separation diagram. Monotonic envelope (continuous blue line), elastic unload (dashed blue line).

Based on the mechanical response chosen in Figure 1, the evolutions of the three different energies associated with a loading-unloading tensile testing are shown in Figure 3. The deformation, elastic, and dissipated energies are plotted in green, blue, and red respectively. The deformation energy w_{def} is naturally the sum of the dissipated w_d and elastic w_e energies *Eq.*(6) since the damage is supposed to be the only microstructural transformation which is fully dissipative during loading, see *Eq.*(11) (no energy storage is induced by the microstructural transformations). Figure 3(a) illustrates that during the elastic unloading w^d_e remains constant (no evolution of damage) while w_e returns to zero. In parallel, the deformation energy w_{def} also decreases and tends towards the energy previously dissipated during the first loading cycle, w^d_d. In Figure 3(b) the elastic reloading while $u \leq u_d$ is shown (dashed lines) and extended by a monotonic loading until rupture for $u_d = u_c$ (full lines).

Under these restrictive assumptions, the area under the traction-separation curve, Figure 1 (equivalent to a monotonic traction rupture) is completely dissipated when the cohesive zone vanishes. In the next sub-section once the thermodynamic working framework has been specified, this important property is discussed. Then, another point to underline is that if the traction-separation curve is classically considered as the constituent element of the behavior of the cohesion zone, it is thus the same for the evolutions of $w^d_{def}(u_d)$ and $w^d_e(u_d)$. Therefore, instead of using the tension-separation curve to describe the damage progress, associated with the loss of stiffness, it is also possible to use the evolution of the allowable maximum elastic energy w^d_e to define the threshold function associated with the damage rate.

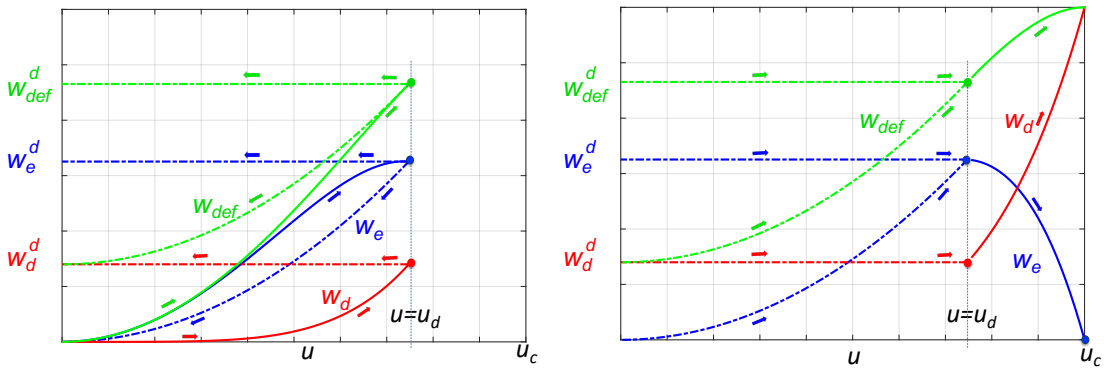

(a) Loading up to $u = u_d$ and unloading. **(b)** Reloading until rupture.

Figure 3: Energy balance evolution during a load-unload-reload process - Continuous lines are associated with the monotonic envelope, dashed lines correspond to the elastic unload and reload.

2.3 Thermodynamics aspects

In this sub-section, the above results and comments are integrated into the TIP framework.

2.3.1 Cohesive zone potential and state laws

In the case of isothermal transformations, the chosen state variables are (u, u_d). A first gambling of the thermomechanical approach is to assume the existence of a potential $\psi(u, u_d)$ capable of gathering all the state laws. Here we identify this potential to the elastic energy w_e defined in *Eq.*(10):

$$\psi(u, u_d) = \frac{1}{2}K(u_d)u^2 \,. \tag{12}$$

The state laws are by construction the partial derivatives of the potential with respect to the state variables. We then define the conjugate variable f^r, associated with u which represents the reversible part of the traction force, and A_d the conjugate variable associated with u_d respectively :

$$\begin{cases} f^r &= \frac{\partial \psi}{\partial u} &= K(u_d)u \\ A_d &= \frac{\partial \psi}{\partial u_d} &= \frac{1}{2}K'(u_d)u^2 \end{cases} , \tag{13}$$

where $K'(u_d) = \frac{\mathrm{d}K(u_d)}{\mathrm{d}u_d}$.

2.3.2 Clausius-Duhem inequality

The irreversibility of the mechanisms accompanying the opening of the cohesive zone is depicted by the Clausius-Duhem inequality which enables the definition of the intrinsic dissipation w^o_d . In the present framework, it can be written as :

$$w^o_d = w^o_{def} - \dot{\psi} = f\dot{u} - \frac{\partial \psi}{\partial u}\dot{u} - \frac{\partial \psi}{\partial u_d}\dot{u_d} = f^{ir}\dot{u} + X_d\dot{u_d} \geq 0 \,. \tag{14}$$

The terms w_d^o and w_{def}^o determine the dissipated and deformation energy rates, respectively. The symbol $(-)^o$ is introduced to underline that w_d and w_{def} are not a priori state functions and are then path dependent. *Eq.*(14) also introduce the irreversible part of the traction force, $f^{ir} = f - f^r$, and the thermodynamic force X_d associated with $\dot{u_d}$. Note that during an irreversible transformation $\dot{u_d} > 0$ we get $X_d = -A_d$. If damage is the only irreversible process, no dissipation has to be associated with $\dot{u}$. In such a case the irreversible traction force vanishes $f^{ir} = 0$. The traction force f can then be directly defined via the state law:

$$f = f^r = K(u_d)u \, . \tag{15}$$

Moreover, the intrinsic dissipation becomes with *Eq.*(13) and *Eq.*(14) :

$$w_d^o = X_d \dot{u_d} = -\frac{1}{2}K'(u_d)u^2\dot{u_d} \geq 0 \, . \tag{16}$$

The fact that $\dot{u_d} \geq 0$ implies $K'(u_d) \leq 0$ what is physically consistent. The irreversible nature of damage leads to a degradation of the secant stiffness.

2.3.3 Threshold function and damage evolution law

In the TIP framework the thermodynamic forces are supposed to be function of the state variable rates. In the case of the linear TIP proposed by Onsager Onsager 1931, the correspondence between thermodynamic forces and state variable fluxes is linear. The Onsager matrix is supposed to be symmetric positive definite in order to verify the Clausius-Duhem inequality (positive dissipation) whatever the thermodynamic process. Extension to non-linear theory exists as for example the formalism of Generalized Standard Materials Halphen et al. 1975. Based on the hypothesis of normal dissipation, the thermodynamic forces derive from a convex dissipation potential or equivalently, state variables rates derived from a dual dissipation potential, function of the thermodynamic forces. This dissipation potential can also involve the state variables of the model as parameters Lemaitre 1996. A common approach is then:

- to define a threshold function depending on the thermodynamic forces (and possibly state variables)
- to write that irreversibility occurs and develops if the thermodynamic state is on the threshold and remains on it during a time increment.

Note that once the state laws (derived from the thermodynamic potential) and complementary laws (derived from the dissipation potential) have been written, it is then possible to deduce the evolution of the energy balance associated with the transformation.

In what follows in as much as our approach is directly based on the energy balance form imposing by construction non-negative dissipation, the existence of the threshold function will not be associated with the normal dissipation hypothesis. Indeed, the current elastic domain is characterized by $w_e^d(u_d)$ the

maximum elastic energy available for a given damage state which also corresponds to the energy required to further damage the material. Then the damage energy criterion based on the energy balance is defined by :

$$w_e(u,u_d) \leq w_e^d(u_d)\ . \tag{17}$$

The evolution law for u_d is then derived from the fact that for the damage to occur the maximum elastic energy allowable in the material has to be and remain on the threshold during the loading step, i.e.

$$\left\{\begin{array}{lcll} w_e(u,u_d) & = & w_e^d(u_d) & \text{(a)} \\ \dot{w}_e(u,u_d) & = & \dot{w}_e^d(u_d) & \text{(b)} \end{array}\right. . \tag{18}$$

The first equality gives naturally $u_d = u$. The second equality leads to a proposal of evolution equation for the damage :

$$\dot{u}_d = \left\{\begin{array}{llllll} \dot{u} & \text{if} & u = u_d & \text{and} & \dot{u} \geq 0 \\ 0 & \text{if} & u < u_d & \text{or} & \dot{u} \leq 0 \end{array}\right. , \tag{19}$$

what is consistent if we remind the definition of the damage state variable *Eq.*(4) and the fact that the damage increases irreversibly, $\dot{u}_d \geq 0$.

To be fully compatible with non-linear TIP framework, the final step is to propose a threshold function that takes the thermodynamic force X_d into account. As previously stated, we consider a derivative form of the energy balance to get this threshold function *Eq.*(18)b. By using *Eq.*(13) and *Eq.*(16), we get:

$$\frac{d\,w_e}{dt} = -X_d\,\dot{u}_d + K(u_d)u\,\dot{u}\ . \tag{20}$$

On the threshold, *Eq.*(20) becomes :

$$\frac{d\,w_e^d}{d\,u_d}\dot{u}_d = \left(-X_d + K(u_d)u_d\right)\ \dot{u}_d\ . \tag{21}$$

Then a threshold function F involving the thermodynamic force X_d and the state variables can be taken under the form :

$$F(X_d;u,u_d) = K(u_d)u - X_d - \frac{d\,w_e^d}{d\,u_d} \leq 0\ . \tag{22}$$

To be consistent with the incremental form of the energy balance, the equality $F(X_d; u, u_d) = 0$, gives once again $u_d = u$ while the consistency condition $dF = 0$ leads to $du = du_d$, or equivalently to *Eq.*(19).

To be precise, the full calculation of $dF = 0$ at $u = u_d$ leads to:

$$(K(u_d) + 2\,K'(u_d)u_d)\,(du - du_d) = 0\,, \tag{23}$$

then $du = du_d$, except possibly when $u_d = -\frac{K(u_d)}{2\,K'(u_d)}$.

2.3.4 Some comments about the damage evolution equations

To depict the evolution of damage, in addition to the traction-separation curve data, the literature often proposes a specific evolution equation in the form of $\dot{D} = \dot{D}(f, D, \dot{u})$ whatever the definition of the damage variable D Roe et al. 2003; Bouvard et al. 2009; Kuna et al. 2015.

In the foregoing, because of the hypotheses explicitly made on the energy balance (i.e. damage is the only dissipative mechanism and it is totally dissipative), the damage evolution law is fixed by the definition of the damage variable itself and by the explicit form of the energy balance. Note that the damage evolution law *Eq.*(19) deduced from the energy criterion *Eq.*(18) is perfectly compatible with the definition of the damage variable itself given in *Eq.*(4). We can also note that this evolution law is an extremely simple form of the general equation proposed by Roe et al. 2003 , but here this law is totally imposed by the shape of the traction-separation curve or equivalently by the threshold $w_e^d(u_d)$ of *Eq.*(10)

To set ideas, let's consider the following simple case: let $f(u)$ be a 1D traction-separation law. We suppose that the elastic energy is, as often, written as: $\psi(u, D) = (1 - D)K_0\frac{u^2}{2}$, where D is the isotropic damage variable, u the displacement jump, and K_0 the elastic stiffness of the virgin cohesive zone. We consider a monotonic loading. The deformation energy rate is given by definition:

$$(w_{def})^0 = f(u)\frac{du}{dt}$$

where $f(u)$ follows the traction-separation curve. The elastic energy rate can be split in two parts:

$$(w_e)^0 = (1 - D)K_0 u\frac{du}{dt} - K_0\frac{u^2}{2}\frac{dD}{dt}$$

If we assume now that the damage is the only irreversible mechanism, then the traction force is the conjugate variable of the displacement jump, where $f(u) = \frac{\partial\psi(u,D)}{\partial u} = (1 - D)K_0 u$ and $(w_e)^0 = (w_{def})^0 - K_0\frac{u^2}{2}\frac{dD}{dt}$ If now the damage is supposed to be exclusively dissipative (no internal stored energy), then the dissipation is given by:

$$(w_d)^0 = K_0\frac{u^2}{2}\frac{dD}{dt} = (w_{def})^0 - (w_e)^0$$

Following the traction-separation curve, the damage evolution has to verify:

$$\frac{dD}{dt} = 2\frac{\left[(w_{def})^0 - (w_e)^0\right]}{K_0 \frac{u^2}{2}}$$

Noting that for each current point $(u, f(u))$ of the traction separation curve, we have $w_e = \frac{1}{2}f(u)u$, the time derivation, following the curve, reads :

$$(w_e)^0 = \frac{1}{2}f(u)\frac{du}{dt} + \frac{1}{2}\frac{df(u)}{dt}u$$

Then,

$$\frac{dD}{dt} = \frac{f(u)\frac{du}{dt} - \frac{df(u)}{dt}u}{K_0 \frac{u^2}{2}}$$

The right-hand member of this equation is fully determined by the traction-separation curve. Any form of damage evolution law, incompatible with this previous equation, would lead to an energy balance form incompatible with the initial energy assumptions (i.e. form of the free energy, damage unique and exclusive dissipative mechanism). The consequences could be the appearance of energy storage mechanisms, i.e. $\dot{w}_d^d < \dot{w}_{def}^d - \dot{w}_e^d$, or internal energy transformation into dissipated energy (release of stored energy), i.e. $\dot{w}_d^d > \dot{w}_{def}^d - \dot{w}_e^d$. Taking into account this stored energy variations should lead to the introduction of new internal state variables and/or to a change of the deformation energy rate definition Fremond 2002.

3 3D cohesive zone model

In this paragraph, we propose an extension to a 3D vectorial version of the CZM where the isotropic damage is controlled by the evolution of the maximum recoverable elastic energy, $w_d^e(u_d)$. Isotropic damage means here that a scalar state variable is solely used to describe the damage evolution. This generalization has been made by following the same approach as the one previously proposed, namely define a damage variable and a energy balance where the damage is the only dissipative phenomenon.

3.1 Mechanical variables

Regarding the mechanical description of the cohesive zone, the traction force and the separation become now vectors. Let us introduce a frame of reference where directions 1 and 2 correspond to the tangent plane of the cohesive zone while direction 3, is the normal direction. The traction vector, $\mathbf{f}$, whose components are (f_{t_1}, f_{t_2}, f_n) and the separation vector, $\mathbf{u}$, which has 3 components denoted by (u_{t_1}, u_{t_2}, u_n) are introduced. As is conventionally admitted in CZM, the normal move jump denoted by u_n is positive or null. This unilateral condition is taken into account by a Signori type relationship in the numerical simulations, using the open source software LMGc90 Dubois et al. 2006, performed at the end of this article.

3.2 Cohesive zone potential and state equations

A set of state variables has first to be chosen. Here we selected the components (u_{t_1}, u_{t_2}, u_n) of the separation vector and a scalar damage variable denoted by u_d. Then, to generalize the form of the cohesive zone potential proposed in *Eq.*(12), the following form, inspired by Bouvard et al. 2009, is adopted :

$$\begin{aligned} \psi(\mathbf{u}, u_d) &= w_e(\mathbf{u}, u_d) \\ &= \tfrac{1}{2}\left(K_n(u_d)u_n^2 + K_t(u_d)u_{t_1}^2 + K_t(u_d)u_{t_2}^2\right) \\ &= \tfrac{1}{2}K_n(u_d)(u_n^2 + \alpha u_{t_1}^2 + \alpha u_{t_2}^2) \\ &= \tfrac{1}{2}K_n(u_d)u_{eq}^2 \end{aligned} \quad , \tag{24}$$

where:

$$u_{eq} = (u_n^2 + \alpha u_{t_1}^2 + \alpha u_{t_2}^2)^{\frac{1}{2}} \ . \tag{25}$$

The parameter α is the ratio between $K_t(u_d)$, the tangential and $K_n(u_d)$, the normal secant stiffnesses at a given u_d. In the case of isotropic damage α is a constant.

In *Eq.*(26), a 3D formulation of the scalar depicting the isotropic damage is given. By construction, u_d takes the 3D aspect of the separation vector $\mathbf{u}$ into account and then $\dot{u}_d$ is non-negative and de facto respects the irreversibility of the damage progress.

$$u_d = \max\left\{u_{eq}(\tau), \forall \tau \leqq t\right\} \ . \tag{26}$$

By definition, the state laws are the partial derivatives of the cohesive zone potential *Eq.*(24). They introduce the components of the reversible traction vector $\mathbf{f}^r$ and the conjugate variable A_d associated with (u_{t_1}, u_{t_2}, u_n) and u_d respectively :

$$\left\{\begin{array}{lllll} f_n^r &= \frac{\partial \psi}{\partial u_n} &= K_n(u_d)u_n & & \\ f_{t_1}^r &= \frac{\partial \psi}{\partial u_{t_1}} &= \alpha K_n(u_d)u_{t_1} &= K_t(u_d)u_{t_1} & \\ f_{t_2}^r &= \frac{\partial \psi}{\partial u_{t_2}} &= \alpha K_n(u_d)u_{t_2} &= K_t(u_d)u_{t_2} & \\ A_d &= \frac{\partial \psi}{\partial u_d} &= \tfrac{1}{2}K'(u_d)u_{eq}^2 & & \end{array}\right. \ . \tag{27}$$

Because only damage induces irreversibility, no dissipation has to be associated with the component of the separation vector. The reversible part $\mathbf{f}^r$ of the separation can therefore be identified with $\mathbf{f}$, then $\mathbf{f} = \mathbf{f}^r$.

3.2.1 Energy definition of the damage threshold

To extend the damage energy criterion to a 3D isotropic damageable CZM, it is possible to choose the damage variable, u_d, whose evolution is directly related to that of the elastic energy w_e^d. In the 3D case, this maximun elastic energy, for a given damage state u_d, describes in the displacement space a half spheroid of radii $r_n(u_d) = \left(\frac{2w_e^d(u_d)}{k_n(u_d)}\right)^{\frac{1}{2}}$ and $r_t(u_d) = \left(\frac{2w_e^d(u_d)}{\alpha\, k_n(u_d)}\right)^{\frac{1}{2}} = \frac{r_n(u_d)}{\sqrt{\alpha}}$ as shown in Figure 4. As the normal jump denoted u_n is by definition positive or null only half of the spheroid is reachable for any separation states.

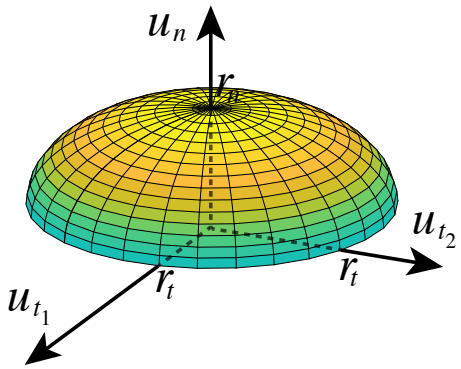

Figure 4: 3D representation of the reachable separation states for a given damage state u_d . The color variation represents the value of u_n.

As long as the further separation states, $\mathbf{u}$, respect the damage energy criterion (i.e. $w_e(\mathbf{u}, u_d) < w_e^d(u_d)$), the behavior remains elastic. Then for a given opening such that $u_{eq} = u_d$, the elastic energy reaches the maximal value associated with this damage state (i.e. $w_e(\mathbf{u}, u_d) = w_e^d(u_d)$). Once the surface of the spheroid is reached:

- either the separation increment $\delta\mathbf{u}$ is directed towards the inside of the spheroid, and an elastic unloading at constant damage can be observed,
- or $\delta\mathbf{u}$ is directed towards the outside of the spheroid, and then the damage develops defining a new elastic limit surface.

For isotropic damage, a single evolution equation for u_d is required. We have already underlined that for threshold behavior law, the yield function depends on the thermodynamic forces and possibly on the states variables themselves, acting as parameters. In the present case, the thermodynamic force of the model , associated with the damage variable rate, is X_d. A generalized form of the yield criterion proposed in *Eq.*(22) is chosen where the role of u used in the 1D scenario is played by u_{eq}. So, the proposed yield energy criterion *Eq.*(17), may be rewritten using the thermodynamic force, X_d as:

$$F(X_d; u_{eq}, u_d) = K_n(u_d)\, u_{eq} - X_d - \frac{d\, w_e^d}{d\, u_d} \leq 0\,. \tag{28}$$

Damage develops if the threshold is reached, $F(X_d; u_{eq}, u_d) = 0$ and if the consistency condition is verified, $\dot{F}(X_d; u_{eq}, u_d) = 0$. For the same reasons as the ones shown for the 1D model, the evolution law of

the parameter u_d is written as:

$$\dot{u}_d = \dot{u}_{eq} \text{ if } u_d = u_{eq} \text{ and } \dot{u}_{eq} \geq 0 \,, \tag{29}$$

results which, as already underlined, are imposed by the very definition of the damage variable.

An illustration of the energy criteria is given in Figure 5. Following a monotonic loading (i.e. remaining on the $w_e^d(u_d)$ curve), $K_n(u_d)u_d$ is the slope of the deformation energy w_{def}^d, X_d is the slope of the dissipated energy w_d^d and $(w_e^d)'$ is naturally the slope of the maximal allowable elastic energy w_e^d.

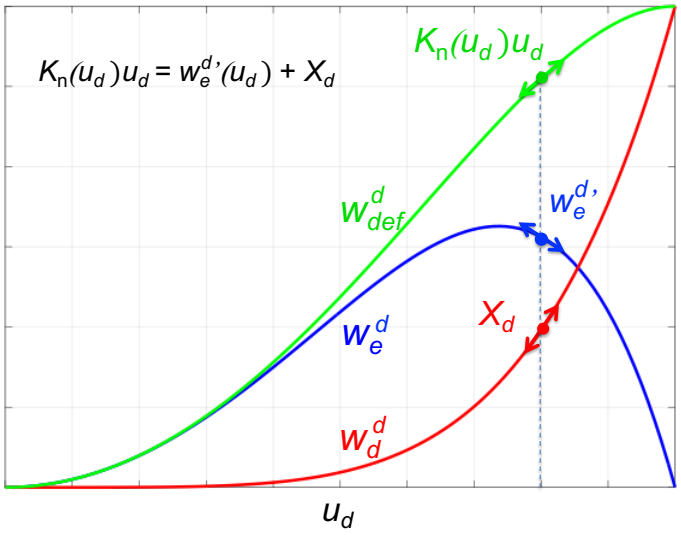

Figure 5: Illustration of the damage energy criterion - $u_{eq} = u_d$

To conclude section 3, we would like to stress once more the fact that the damage evolution law is not here a matter of choice. It is imposed by the chosen form of the energy balance and by the definition of the damage state variable.

The state equations Eqs(27) and the evolution equation *Eq.*(29) will be, in what follows, implemented in a home-made finite element code. The different material parameter of the constitutive equations will be specified. In order to show the capabilities of such a CZM, two types of simulations are made here after. The first one is a bending test whose numerical results are compared with experimental one's. The second one is a Brazilian disc test whose the material is made of heterogeneous elastic grains.

4 Numerical Implementation

To illustrate the potentiality of the proposed model, simulations reproducing a common benchmark extracted from the literature Galvez et al. 1996 were carried out. It is important to notice that the objective of this practical comparison is simply to show the operability of the model and not to optimize its parameters in order to fit the benchmark. The numerical implementation of the previous model is then done in the code LMGc90 based on Non-Smooth Contact Dynamics (NSCD) Moreau 1988; Jean 1999; Jean

et al. 2001. The NSCD method is dedicated to solving problems related to dynamic systems with unilateral constraints. It is therefore particularly suitable for contact friction problems. It proposes a non-smooth treatment (no compliance, no penalty) of the conditions of contact Jean 1999, which is explicit in the definition of u_n. The way which adhesion is taken into account in this method makes it possible to consider each point of contact as a cohesive zone. Then the mechanical behavior of the cohesive zones may vary at any point of the spatial discretization of the problem. This relevant modeling framework was then adopted to numerically simulate crack propagation with cohesive zone Champagne et al. 2014 .

4.1 Bending test

To compare the proposed model with a benchmark found in literature Galvez et al. 1996, the form of the maximum storable elastic energy, which we remember is $w_e^d(u_d)$, must be specified in order to be able to implement it in LMGc90 , the open source platform [1] used to carry out the simulations Dubois et al. 2011. This benchmark, illustrated Figure 6, traces the evolution of a crack in mixed mode to be followed. In the context of this feasibility study, a simple quadratic form of $w_e^d(u_d)$ is proposed. In what follows, we also assumed the existence of a pure elastic domain and thus the existence of a threshold equivalent elastic deplacement u_{eq}^e, simply denoted by u_e. The maximum storable elastic energy as a function of the damage parameter u_d simply reads:

$$w_e^d(u_d) = A\,(u_d - u_c)^2 + B\,(u_d - u_c)\,, \text{ if } u_e \leq u_d \leq u_c \quad , \tag{30}$$

where u_c is the critical equivalent displacement corresponding to the crack onset. Parameters A and B are two constants chosen to ensure the C_1 continuity of the maximum storable elastic energy, $w_e^d(u_d)$, at the threshold equivalent elastic deplacement, $w_e^d(u_e) = \frac{1}{2}\,K_n^0\,u_e^2$. They are defined by:

$$\begin{cases} A = -\frac{1}{2}\,K_n^0\,u_e\,\frac{(2u_c - u_e)}{(u_c - u_e)^2} \\ B = -K_n^0\,\frac{u_c u_e}{u_c - u_e} \end{cases} , \tag{31}$$

where K_n^0 is the initial normal stiffness of the CZM.

The thickness of the sample, denoted by H, is equal to 0.3 m while its length is equal to 1.2 m. A 0.15 m pre-crack is located in the middle on the lower edge. The point B is fixed in both x and y directions whereas the point A is only fixed in the y direction. A displacement is imposed on the point A to load the structure. .The mesh is composed of 3 parts: Two coarse meshes, the left and the right parts of the structure composed respectively of 958 and 2 063 T3 elements, where no interface elements have been introduced between the different meshes and a finer mesh, assuring the continuity of the structure (domain Ω_1 in Figure 6), composed of 6 723 T3 elements where the crack path is supposed to appear and where

[1] https://git-xen.lmgc.univ-montp2.fr/lmgc90/

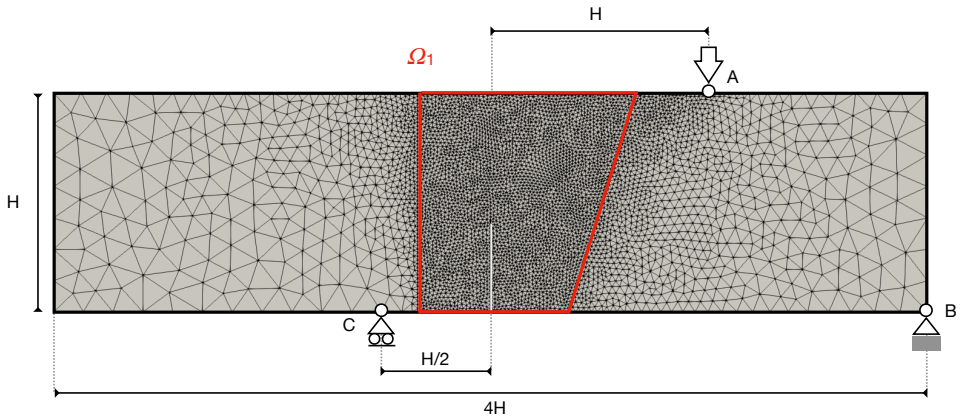

Figure 6: Characteristics of the benchmark issued from Galvez et al. 1996 used for simulation

K_n^0 (N m^{-1})	α	u_e (m)	u_c (m)
2.48 10^9	0.5	0.5 10^{-6}	1.5 10^{-6}

Table 1: Parameter values of the CZM

interface elements are therefore introduced between each element. The interactions between elements of Ω_1 are governed by the proposed cohesive zone model where the initial secant elastic stiffness, K_n^0 and K_t^0, are chosen to satisfy the criterion proposed in Blal et al. 2011 to limit the reduction of stiffness due to the presence of CZM. It is important to underline that the objective of this practical comparison is simply to show the operability of the model and not to optimize its parameters in order to fit the benchmark. The values of the CZM parameters are summarized in Table1.

Figure 7 shows the evolution, for different simulation times, of different characteristic quantities associated with the model : the damage variable, the elastic energy w_e and the dissipated energy w_d. In order to present a quantity varying from 0 to 1 the damage ratio, as a function the damage variable, is introduced and defined by $\frac{<u_d-u_e>^+}{u_c-u_e}$. To improve the visibility of these different quantities supported by the interfaces, they are projected on adjacent elements.

Figure 7(a), corresponding to a pre-cracking state, shows a concentration of the elastic energy at the outset of the crack tip. However, the damage criterion has not been reached within the cohesive zone so that no damage or dissipation has yet occurred (see *Eq.*(17)). The corresponding map to $\frac{<u_d-u_e>^+}{u_c-u_e}$ and w_d are then uniformally egal to 0. As expected, Figure 7 (b) and (c), corresponding to two post-cracking steps, highlight the correlation between the evolution of the dissipated energy and the damage ratio. The elastic energy is still concentrated ahead of the crack tip, then returns to zero along the crack lips. In contrast, the dissipated energy related to the damage evolution can be exhibited all along the crack path. Similarly, the damage field allows the cracking path to be tracked.

To exhibit the capability of our CZM where only the shape of the cohesive energy associated with a simple energy balance is needed (cf. *Eq.*(30)), different quantities, numerically obtained, are compared with experimental measurements present in the literature Cendón et al. 2000. For such comparisons, Figure 8 presents both the classical crack path monitoring and the load vs. CMOD curve (Crack Mouth Opening Displacement).

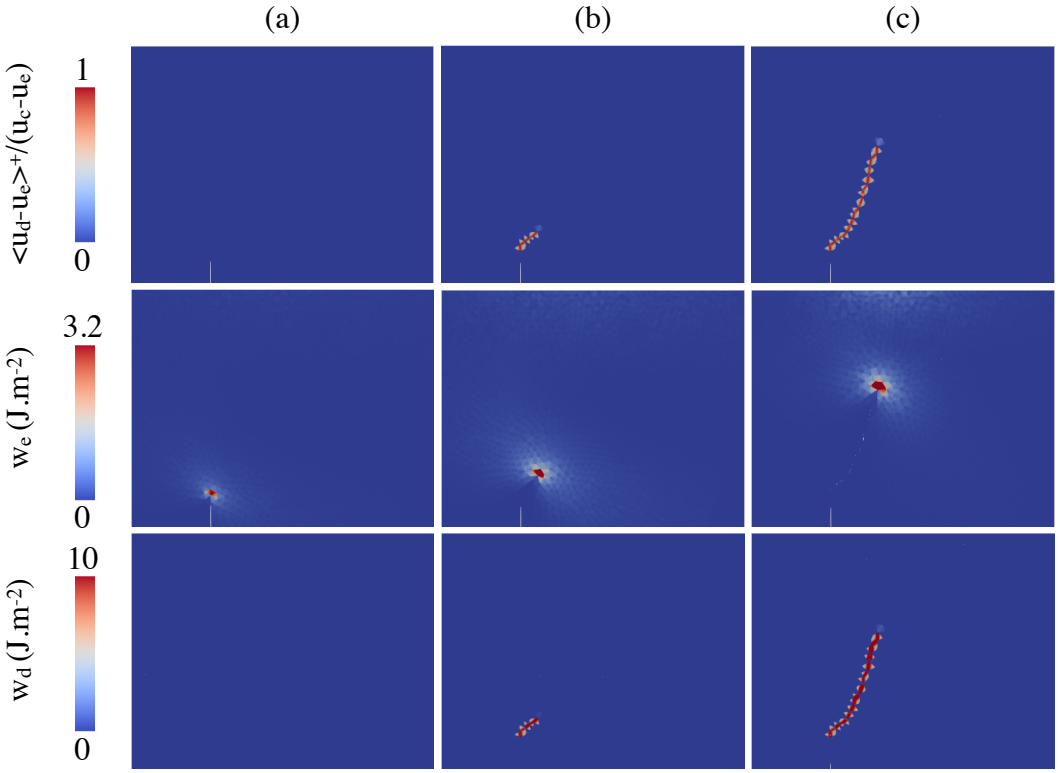

Figure 7: Visualization of the damage ratio (top row), the elastic energy (center) and the dissipated energy (bottom row) during the crack propagation

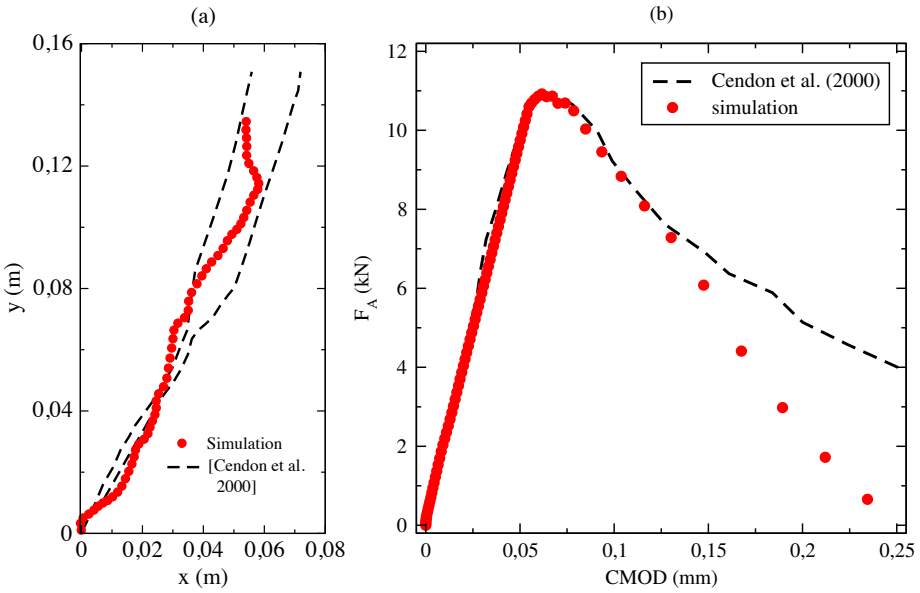

Figure 8: Comparison of numerical macroscopic measurements associated to the crack evolution with experimental results Cendón et al. 2000: a) The crack path and b) the load vs. CMOD curve.

In Figure 8(a) and Figure 8(b), the red dot line corresponds to the simulation result while the black dashed lines represent the crack envelop obtained experimentally Cendón et al. 2000. In Figure 8a, the crack obtained numerically corresponds closely to the experimental envelope. The starting angle is strongly related to the discretization around the initiation point, explaining the slight difference at the beginning of the initiation. Then, the path is corrected and repositioned in the experimental envelope until the end of the simulation.

Concerning the force vs. CMOD curves, they fit perfectly in the section corresponding to the linear increase. This highlight that the introduction of a 2D interface element, where the values of K_n^0 and K_t^0 satisfy the criterion proposed in Blal et al. 2011 between each elements of Ω_1 do not affect the global stiffness of the sample. The maximum force obtained is also in good agreement with that obtained in the experiment, as well as the beginning of the non-linear decreasing part of the CMOD curve occurring at the initiation of cracking. In the last part, the curves diverge. This difference is partly explained by the fact that the numerical simulation is two-dimensional while the experiments are three-dimensional. Indeed, not all deformation modes are taken into account (especially out-of-plane modes), which explains this different behavior at the end of the simulation. Moreover, we have arbitrarily chosen a 2nd degree polynomial to characterize the damage of the cohesive zone model, *Eq.*(30). This choice could be fine-tuned in order to better account for experiences by taking a Needleman-type damage, Bosch et al. 2006; Needleman 1990.

4.2 Sensitivity study

Finally, in order to see the impact of a variation in the parameters u_e and u_c on the overall behavior of the system and more particularly on the evolution of the force vs. CMOD curves, a sensitivity study is proposed. The influence of these parameters on the crack path is not presented because it is not very significant. The influence of these parameters on the energy available to be dissipated in the model is pointed out in Figure 9. The parametric study is carried out relative to the reference point $(0, 0)$ corresponding to the results presented in Figure 8(b) with the parameters define in table 1. With the chosen law, a variation of u_c has almost the same consequence as a variation of u_e in terms of the energy available to be dissipated. Then the map presented in Figure 9 is symmetric in the regard of the circle-triangle diagonal. During the different parametric studies, the color code used for the curves will refer to the one defined in Figure 9.

Figure 10 presents the normalized plots of $w_e^d(u_d)$ for different values of u_e and u_c (Figure 10(a)) and the corresponding force vs. CMOD curves (Figure 10(b)). The normalization parameters are $u_{e,0} = 0.5\,10^{-2}$ and $w_{e,0} = w_{e,0}^d(u_{e,0})$ using the values of parameters in Tab. 1. Even if the shape of the curves is significantly different in Figure 10 (a), the energies available to be dissipated for the case represented by a cross and the one represented by a square are of same order of magnitude. The maxima order observed at the scale of the CZM models (Figure 10(a)) is conserved at the scale of the structure (Figure 10(b)).

In Figures 11 to 13, we observe respectively the influence of u_c and u_e on the force vs. CMOD curves. These figures show that the influence of the variation of u_c is less than that of u_e. Indeed, where we

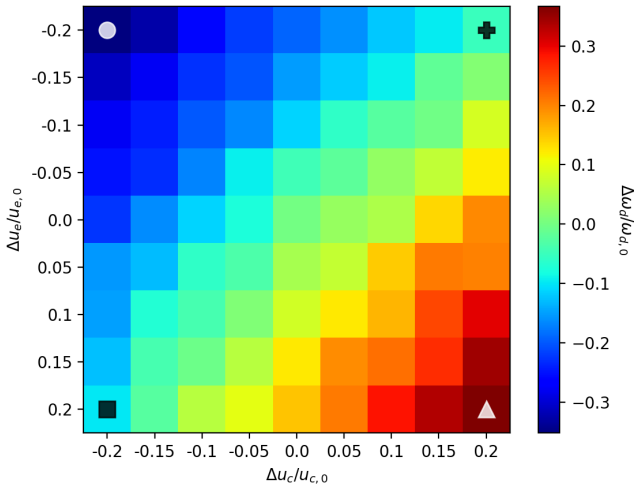

Figure 9: Map of the normalized dissipated energy variations as a function of the variations of u_e and u_c. The symbols used at the four corners of the map identify the curves shown in Figure 10.

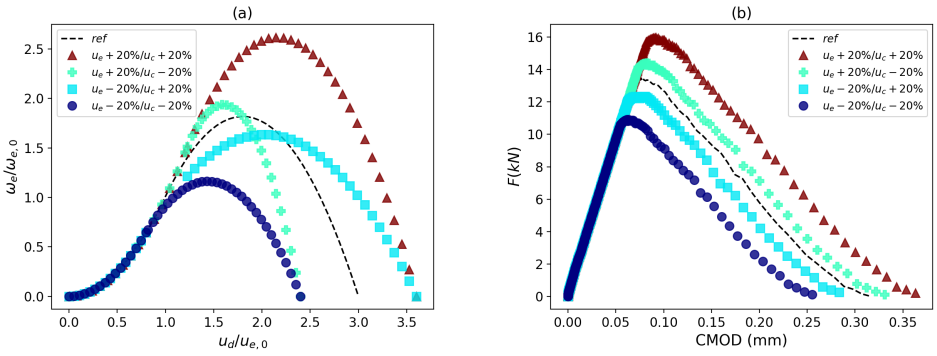

Figure 10: (a) Normalized plots of $w_e^d(u_d)$ for different values of u_e and u_c. The normalization parameters are $u_{e,0} = 0.5\,10^{-2}$ and $w_{e,0} = w_{e,0}^d(u_{e,0})$ using the values of parameters in Tab.1. (b) Corresponding force vs. CMOD curves.

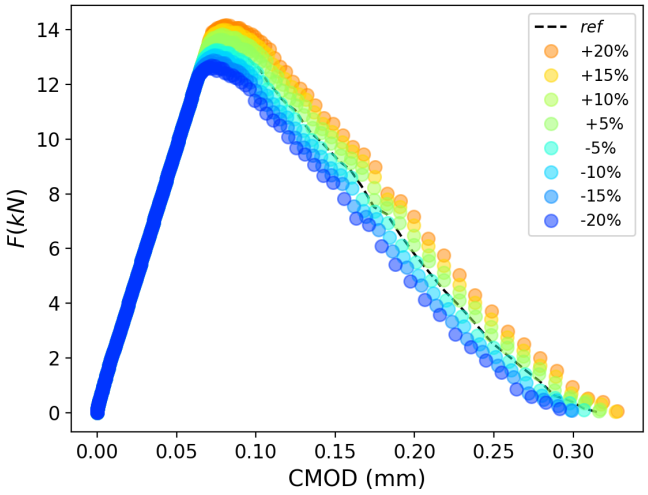

Figure 11: Comparison between the reference Load vs. CMOD curve (dash line) and the ones related to the variation of u_c of ±20% while u_e constant.

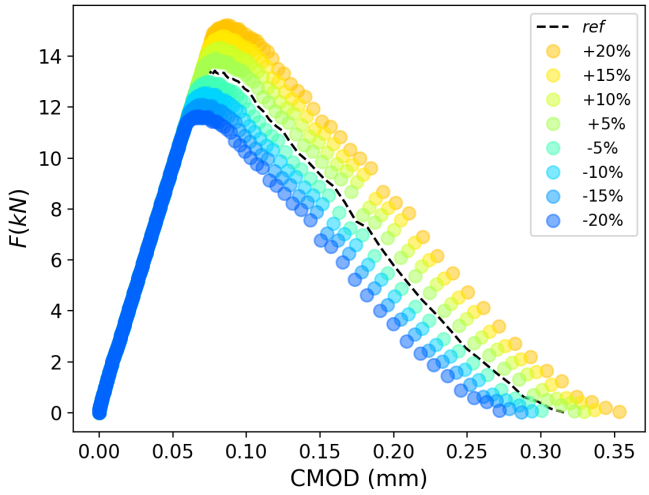

Figure 12: Comparison between the reference Load vs. CMOD curve (dash line) and the ones related to the variation of u_e of ±20% while u_c constant.

observe for a variation of u_c a variation of less than 10% on the critical values of the curve (F_{max} and $CMOD_{max}$), while a variation of more than 20% for an equivalent variation of u_e is observed. Nevertheless, in both cases, an increase of the damage energy w_d induces an increase of the CMOD and loading maxima in the Load vs. CMOD curve. In this model where an elastic domain is assumed, u_e is the threshold where the damage begins to occur. This value determines the outset of the non-linear response of the structure. This is exhibited in Figure 12 where an increase of u_e at the local scale induces an increase of the maximal force at the macroscopic scale and a delay of the occurence of the nonlinear response of the curves.

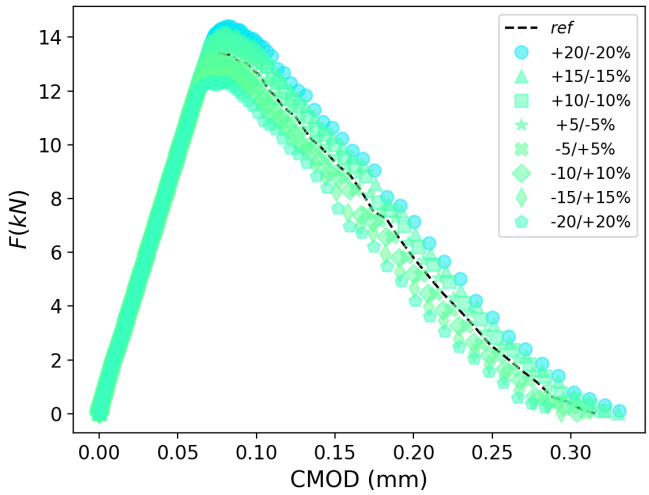

Figure 13: Comparison between the reference Load vs. CMOD curve (dash line) and the ones related to the variation of u_c and u_e of ±20% while w_d^o is constant.

Figure 13 demonstrates that the non-linear region of the curve is also governed by the shape of the energy curve (cf. Figure 10). Although the dissipative energy in this parametric study is almost constant, we observe a variation of about 10% on the characteristic values of the response curve. So by combining the effects of u_e, u_c and the shape of the local curve (cf. Figure 10) it is possible to obtain a better optimal

K_n^0 (N m^{-1})	α	u_e (m)	u_c (m)
2.48 10^{15}	0.4	0.8 10^{-6}	1.0 10^{-6}

Table 2: Parameter values of the CZM

result to fit experiments. Thus the experimental characterization of this type of local curve depicting the micro-structural phenomenon linked to fracture is relevant and is still an ongoing problem.

4.3 Brazilian test

As a complement to the previous numerical simulation and as an opening to the continuation of the present work, the developed CZM law is used in the simulation of a Brazilian test. This test consists of compressing a circular sample located between two rigid plates. Contrary to the previous case, no pre-crack is introduced in the numerical model. The microstructure of the sample used is presented on the left side of Figure 14. This microstructure has been generated using the open-source Software Neper Quey et al. 2011. It is composed of 1 000 elastic grains following a normal size distribution to make the microstructure heterogeneous Ma et al. 2018. In these case, the cohesive zones are only introduced at the grain boundaries. The mesh size used for meshing is identical for all grains and calibrated so that the smallest grains have at least two elements on their smallest side. The total number of elements is 98 378. A zoom of the mesh is shown on the right hand side of Figure 14. For the sake of simplicity the diameter of the sample is unitary. A vertical velocity is imposed on both walls to compress the sample. The simulation is carried out in large deformations in order to manage possible strain localisation and grain rotations. The elastic constitutive equations are those of the linear elasticity where stresses and strains are respectively represented by the 2nde Piola-Kirchoff stress tensor and the Green-Lagrange strain tensor.

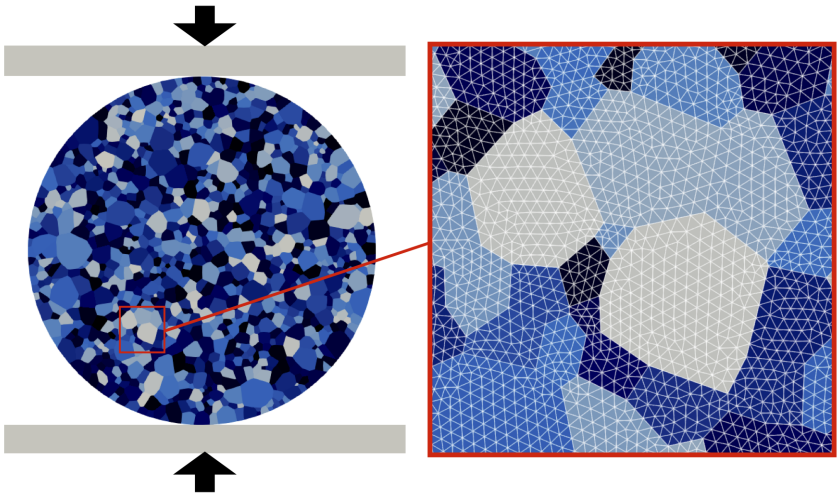

Figure 14: Visulation of the meshed microstructure used in the simulation of the Brazilain disc test

For homogeneous material during Brazilian test a tensile state is induced in the center of the disc perpendicular to the load direction. Increasing the load leads to an increase in tensile stress until a crack appears in the center of the disc. Under the effect of the load, the crack develops until the disc eventually separates into at least two parts. For a heterogeneous material the damage occurs near the rigid plates and

then develops along the loading axis until the disk breaks Na et al. 2017. Figure 15 shows a visual of the sample at the end of the simulation.

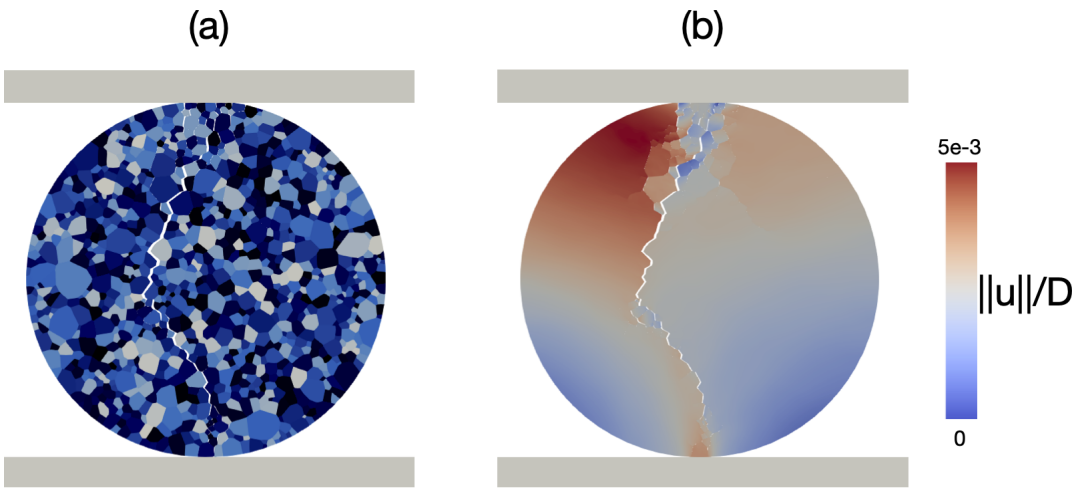

Figure 15: Final state of the simulation: Vizualisation of a) the crack through the microstructure and b) the norm of displacement field normalized by the value, D, of the diameter within the sample.

Figure 15(a) shows the macro crack zigzagging through the microstructure. This extends from the contact between the sample and the rigid plates away from the centre of the sample. Figure 15(b) shows the norm of the adimentionalized displacement field within the sample. The discontinuities within this field allow the observation of multiple cracking paths generated during compression. Numerous disjointed fragments can be particularly seen in the volume near the top wall.

To complete these observations, the evolution of the dissipated energy fields is presented in Figure 16. The image (a) corresponds to the initiation of the crack while the image (f) corresponds to the end of the simulation. The other images are captured at intermediate times. Through the figures 16 (a) to (f) the damage evolution is exhibited where branching is observed until the coalescence of the macro crack. The next step is to experimentally perform the same type of test using an experimental setup coupling kinematic and thermal full-field measurements. The kinematic measurements will allow us to locate zones of strain localization and even discontinuities of the displacement fields while the thermal measurements will be used to determine the zones where the dissipation is localized. The confrontation of this two informations should should help us to check the relevance of this energy approach of cohesive zones.

5 Conclusion

In this paper we present an energy criterion for cohesive zone models where the damage progress is assessed together with the ability of the material to store energy elastically. The damage parameter used is $u_d(t) = Sup\left\{u_{eq}(\tau)\,,\ \tau \leq t\right\}$ where u_{eq} is an equivalent displacement compatible with the isotropic evolution of the damage progress.The paper shows that if damage is the unique and exclusive dissipative mechanisms, the damage evolution law is automatically fixed by the evolution of the maximum storable elastic energy $w_e^d(u_d)$. We have also underlined that the data of this energy is equivalent in a 1D formalism

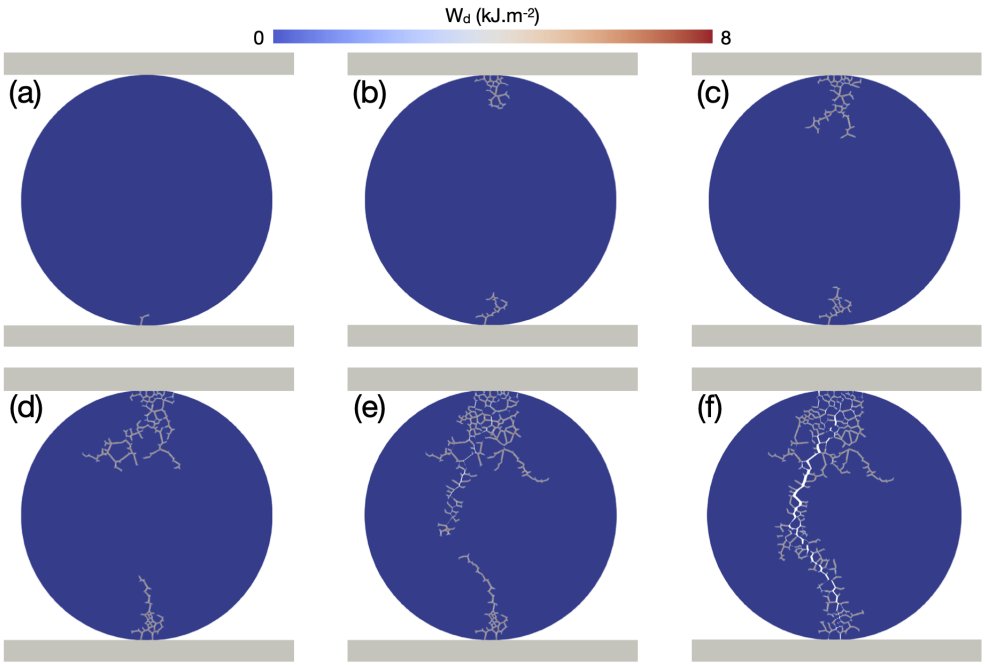

Figure 16: Evolution of the dissipated energy field from the crack initiation (a) to the end of simulation (f).

to the one of a traction-separation law. The interest of this energy approach is its immediate generalization to 3D cohesive zone models. In order to check the operational character of this type of approach, the isotropic damage model has been implemented in the open source software LMGc90 based on Non-Smooth Contact Dynamics (NSCD) and used to perform numerical simulations in the case of bending and Brazilian tests. The results obtained for this plain stress modeling are encouraging. Using a simple quadratic function $w_e^d(u_d)$ for the interface, we obtained a close correlation between the simulations and the experimental observations of the crack path for the bending test, and realistic multicrack propagations in the case of the Brazilian test. A parametric study of the macroscopic response of the structure naturally demonstrates the importance of the shape of the function $w_e^d(u_d)$ which characterize the interface behavior between two elements. It is indeed this quantity that we will have to identify experimentally. In subsequent theoretical developments, first we will consider an extension to a non isotropic degradation of the material elastic properties. From an experimental stand point Brazilain test will be performed by using full field techniques during monotonic loadings, the goal being to extract from the experimental data valuable information on the form of the energy balance and particularly on $w_e^d(u_d)$.

6 Bibliography

Abdelmoula, R., J.-J. Marigo, and T. Weller (2009). "Construction des lois de fatigue à partir de modèleles de forces cohésivesives : cas de fissures en mode I". Comptes Rendus Mécanique 337.3, pp. 166 –172. DOI: https://doi.org/10.1016/j.crme.2009.04.002

Alessi, R., J.-J. Marigo, and S. Vidoli (2015). "Gradient damage models coupled with plasticity: Variational formulation and main properties". Mechanics of Materials 80.Part B. Materials and Interfaces, pp. 351 –367. DOI: https://doi.org/10.1016/j.mechmat.2013.12.005

Alfano, G. and E. Sacco (Oct. 2006). "Combining interface damage and friction in a cohesive zone model". International Journal for Numerical Methods in Engineering 68.5, pp. 542–582. DOI: 10.1002/nme.1728

Allix, O., P. Ladevèze, and A. Corigliano (1995). "Damage analysis of interlaminar fracture specimens". Composite Structures 31.1, pp. 61 –74. DOI: https://doi.org/10.1016/0263-8223(95)00002-X

Amor, H., J.-J. Marigo, and C. Maurini (2009). "Regularized formulation of the variational brittle fracture with unilateral contact: Numerical experiments". Journal of the Mechanics and Physics of Solids 57.8, pp. 1209 –1229. DOI: https://doi.org/10.1016/j.jmps.2009.04.011

Benaarbia, A. and A. Chrysochoos (2017). "Proper orthogonal decomposition preprocessing of infrared images to rapidly assess stress-induced heat source fields". Quantitative InfraRed Thermography Journal 14.1, pp. 132–152. DOI: 10.1080/17686733.2017.1281553. eprint: https://doi.org/10.1080/17686733.2017.1281553

Bernard, P., N. Moës, and N. Chevaugeon (2012). "Damage growth modeling using the Thick Level Set (TLS) approach: Efficient discretization for quasi-static loadings". Computer Methods in Applied Mechanics and Engineering 233-236, pp. 11 –27. DOI: https://doi.org/10.1016/j.cma.2012.02.020

Blal, N., L. Daridon, Y. Monerie, and S. Pagano (2011). "Criteria on the artificial compliance inherent to the intrinsic cohesive zone". Comptes Rendus Mécanique 339.12, pp. 789 –795. DOI: https://doi.org/10.1016/j.crme.2011.10.001

Bosch, M. V. den, P. Schreurs, and M. Geers (2006). "An improved description of the exponential Xu and Needleman cohesive zone law for mixed-mode decohesion". Engineering Fracture Mechanics 73.9, pp. 1220 –1234. DOI: https://doi.org/10.1016/j.engfracmech.2005.12.006

Bouvard, J., J. Chaboche, F. Feyel, and F. Gallerneau (2009). "A cohesive zone model for fatigue and creep-fatigue crack growth in single crystal superalloys". International Journal of Fatigue 31.5, pp. 868 –879. DOI: https://doi.org/10.1016/j.ijfatigue.2008.11.002

Cazes, F. and N. Moës (2015). "Comparison of a phase-field model and of a thick level set model for brittle and and quasi-brittle fracture". Numerical Methods in Engineering 103.2, pp. 114–143

Cendón, D., J. Gálvez, M. Elices, and J. Planas (2000). "Modelling the fracture of concrete under mixed loading". International Journal of Fracture 103.3, pp. 293–310. DOI: 10.1023/A:1007687025575

Chaboche, J., F. Feyel, and Y. Monerie (2001). "Interface debonding models: a viscous regularization with a limited rate dependency". International Journal of Solids and Structures 38.18, pp. 3127 –3160. DOI: https://doi.org/10.1016/S0020-7683(00)00053-6

Champagne, M., M. Renouf, and Y. Berthier (Jan. 2014). "Modeling Wear for Heterogeneous Bi-Phasic Materials Using Discrete Elements Approach". Journal of Tribology 136.2. 021603. DOI: 10.1115/1.4026053. eprint: https://asmedigitalcollection.asme.org/tribology/article-pdf/136/2/021603/6284756/trib_136_02_021603.pdf

Chen, Z., A. Bunger, X. Zhang, and R. G. Jeffrey (2009). "Cohesive zone finite element-based modeling of hydraulic fractures". Acta Mechanica Solida Sinica 22.5, pp. 443 –452. DOI: https://doi.org/10.1016/S0894-9166(09)60295-0

Chrysochoos, A., L. Daridon, and B. Wattrisse (July 2014). "Prediction of damage evolution in bonded material using cohesive zone model". 11th World Congress on Computational Mechanics - 5th European Conference on Comput Barcelone, Spain

Chrysochoos, A. (2012). "Infrared thermography applied to the analysis of material behavior: a brief overview". Quantitative InfraRed Thermography Journal 9.2, pp. 193–208. DOI: 10.1080/17686733.2012.746069. eprint: https://doi.org/10.1080/17686733.2012.746069

Corigliano, A. and M. Ricci (2001). "Rate-dependent interface models: formulation and numerical applications". International Journal of Solids and Structures 38.4, pp. 547 –576. DOI: https://doi.org/10.1016/S0020-7683(00)00088-3

Daridon, L., B. Cochelin, and M. Potier-Ferry (1997). "Delamination and Fiber Bridging Modelling in Composite Samples". Journal of Composite Materials 31.9, pp. 874–888. DOI: 10.1177/002199839703100902. eprint: https://doi.org/10.1177/002199839703100902

Daridon, L., B. Wattrisse, A. Chrysochoos, and M. Potier-Ferry (2011). "Solving fracture problems using an asymptotic numerical method". Computers & Structures 89.5, pp. 476 –484. DOI: https://doi.org/10.1016/j.compstruc.2010.12.001

Dubois, F. and M. Jean (2006). "The non smooth contact dynamic method: recent LMGC90 software developments and application". Analysis and Simulation of Contact Problems. Ed. by P. Wriggers and U. Nackenhorst. Berlin, Heidelberg: Springer Berlin Heidelberg, pp. 375–378. DOI: 10.1007/3-540-31761-9_44

Dubois, F., M. Jean, M. Renouf, R. Mozul, A. Martin, and M. Bagnéris (May 2011). "LMGC90". 10e colloque national en calcul des stru Giens, France, Clé USB

Dugdale, D. (1960). "Yielding of steel sheets containing slits". Journal of the Mechanics and Physics of Solids 8.2, pp. 100 –104. DOI: https://doi.org/10.1016/0022-5096(60)90013-2

Fremond, M. (2002). Non-smooth Thermomechanics. Ed. by Springer. Springer-Verlag Berlin Heidelberg

Galvez, J., M. Elices, G. V. Guinea, and J. Planas (1996). "Crack trajectories under mixed mode and non-proportional loading". International Journal of Fracture 81.2, pp. 171–193. DOI: 10.1007/BF00033181

Halphen, B. and N. Quoc-Son (1975). "Sur les matériaux standards generalisés". Journal de mécanique 14, pp. 39,63

Huon, V., Richefeu, V., Shuang, W., Chrysochoos, A., Monerie, Y., and Wattrisse, B. (2010). "Experimental characterisation of a cohesive zone model using digital image correlation". EPJ Web of Conferences 6, p. 43004. DOI: 10.1051/epjconf/20100643004

Jean, M. (1999). "The non-smooth contact dynamics method". Computer Methods in Applied Mechanics and Engineering 177.3, pp. 235 –257. DOI: https://doi.org/10.1016/S0045-7825(98)00383-1

Jean, M., V. Acary, and Y. Monerie (2001). "Non-smooth contact dynamics approach of cohesive materials". Philosophical Transactions of the Royal Society of London A: Mathematical, Physical and Engineering Sciences 359.1789, pp. 2497–2518. DOI: 10.1098/rsta.2001.0906. eprint: http://rsta.royalsocietypublishing.org/content/359/1789/2497.full.pdf

Kachanov, L. (1986). Introduction to continuum damage mechanics. springer

Kolluri, M., J. P. M. Hoefnagels, J. A. W. van Dommelen, and M. G. D. Geers (2014). "Irreversible mixed mode interface delamination using a combined damage-plasticity cohesive zone enabling unloading". International Journal of Fracture 185.1, pp. 77–95. DOI: 10.1007/s10704-013-9899-z

Kondo, D., H. Welemane, and F. Cormery (2007). "Basic concepts and models in continuum damage mechanics". Revue Européenne de Génie Civil 11.7-8, pp. 927–943. DOI: 10.1080/17747120.2007.9692970. eprint: https://doi.org/10.1080/17747120.2007.9692970

Kuna, M. and S. Roth (2015). "General remarks on cyclic cohesive zone models". International Journal of Fracture 196.1, pp. 147–167

Lé, B., N. Moës, and G. Legrain (2018). "Coupling damage and cohesive zone models with the Thick Level Set approach to fracture". Engineering Fracture Mechanics 193, pp. 214 –247. DOI: https://doi.org/10.1016/j.engfracmech.2017.12.036

Lemaitre, J. (1996). A course on dammage mechanics. springer

Lorentz, E. and S. Andrieux (1999). "A variational formulation for nonlocal damage models". International Journal of Plasticity 15.2, pp. 119 –138. DOI: https://doi.org/10.1016/S0749-6419(98)00057-6

Ma, Y. and H. Huang (2018). "DEM analysis of failure mechanisms in the intact Brazilian test". International Journal of Rock Mechar 102, pp. 109–119. DOI: https://doi.org/10.1016/j.ijrmms.2017.11.010

Marigo, J.-J., C. Maurini, and K. Pham (2016). "An overview of the modelling of fracture by gradient damage models". Meccanica 51.12, pp. 3107–3128. DOI: 10.1007/s11012-016-0538-4

Moës, N., C. Stolz, P.-E. Bernard, and N. Chevaugeon. (Apr. 2011). "A level set based model for damage growth: The thick level set approach". International Journal for Numerical Methods in Engineering 86.3, pp. 358–380. DOI: 10.1002/nme.3069

Moreau, J. J. (1988). "Unilateral Contact and Dry Friction in Finite Freedom Dynamics". Nonsmooth Mechanics and Applications. Ed. by J. J. Moreau and P. D. Panagiotopoulos. Vienna: Springer Vienna, pp. 1–82. DOI: 10.1007/978-3-7091-2624-0_1

Na, S., W. Sun, M. D. Ingraham, and H. Yoon (2017). "Effects of spatial heterogeneity and material anisotropy on the fracture pattern and macroscopic effective toughness of Mancos Shale in Brazilian tests". Journal of Geophysical Research: Solid Earth 122.8, pp. 6202–6230. DOI: https://doi.org/10.1002/2016JB013374. eprint: https://agupubs.onlinelibrary.wiley.com/doi/pdf/10.1002/2016JB013374

Needleman, A. (1990). "An analysis of tensile decohesion along an interface". Journal of the Mechanics and Physics of Solids 38.3, pp. 289 –324. DOI: https://doi.org/10.1016/0022-5096(90)90001-K

Nguyen, O., E. Repetto, M. Ortiz, and R. Radovitzky (2001). "A cohesive model of fatigue crack growth". International Journal of Fracture 110.4, pp. 351–369. DOI: 10.1023/A:1010839522926

Onsager, L. (1931). "Reciprocal Relations in Irreversible Processes. I." Phys. Rev. 37 (4), pp. 405–426. DOI: 10.1103/PhysRev.37.405

Ortiz, M. and A. Pandolfi (1999). "Finite-deformation irreversible cohesive elements for three-dimensional crack-propagation analysis". International journal of numerical method in engineering. 44.9, pp. 1267–1282

Pandolfi, A. and M. Ortiz (2013). "Modeling fracture by material-point erosion". International Journal of Fracture 184.1-2, pp. 3–16. DOI: https://doi.org/10.1007/s10704-012-9788-x

Park, K., G. H. Paulino, and J. R. Roesler (2009). "A unified potential-based cohesive model of mixed-mode fracture". Journal of the Mechanics and Physics of Solids 57.6, pp. 891 –908. DOI: https://doi.org/10.1016/j.jmps.2008.10.003

Pham, K. and J.-J. Marigo (2012). "Damage localization and rupture with gradient damage models". Fracture and structural integrity 19, pp. 5–19

Pijaudier-Cabot, G. and Z. P. Bazant (1987). "Nonlocal Damage Theory". Journal of Engineering Mechanics 113.10, pp. 1512–1533. DOI: 10.1061/(ASCE)0733-9399(1987)113:10(1512)

Quey, R., P. Dawson, and F. Barbe (2011). "Large-scale 3D random polycrystals for the finite element method: Generation, meshing and remeshing". Computer Methods in Applied Mechanics and Engineering 200.17, pp. 1729–1745. DOI: https://doi.org/10.1016/j.cma.2011.01.002

Richefeu, V., A. Chrysochoos, V. Huon, Y. Monerie, R. Peyroux, and B. Wattrisse (2012). "Toward local identification of cohesive zone models using digital image correlation". European Journal of Mechanics - A/Solids 34.Supplement C, pp. 38 –51. DOI: https://doi.org/10.1016/j.euromechsol.2011.12.001

Roe, K. and T. Siegmund (2003). "An irreversible cohesive zone model for interface fatigue crack growth simulation". Engineering Fracture Mechanics 70.2, pp. 209 –232. DOI: https://doi.org/10.1016/S0013-7944(02)00034-6

Roth, S., G. Hütter, and M. Kuna (2014). "Simulation of fatigue crack growth with a cyclic cohesive zone model". International Journal of Fracture 188.1, pp. 23–45. DOI: 10.1007/s10704-014-9942-8

Serpieri, R., E. Sacco, and G. Alfano (2015). "A thermodynamically consistent derivation of a frictional-damage cohesive-zone model with different mode I and mode II fracture energies". European Journal of Mechanics - A/Solids 49, pp. 13 –25. DOI: https://doi.org/10.1016/j.euromechsol.2014.06.006

Suo, Z. and J. W. Hutchinson (1990). "Interface crack between two elastic layers". International Journal of Fracture 43.1, pp. 1–18. DOI: 10.1007/BF00018123

Wojtacki, K., L. Daridon, F. Dubois, N. N. Moës, and Y. Monerie (2015). "Analyse comparative de trois méthodes performantes de simulation numérique de la fissuration". 13e colloque national en calcul des structures - CSMA

Zener, C. (1938). "Internal Friction in Solids II. General Theory of Thermoelastic Internal Friction". Phys. Rev. 53 (1), pp. 90–99. DOI: 10.1103/PhysRev.53.90

Zhou, F. and J. F. Molinari (2004). "Dynamic crack propagation with cohesive elements: a methodology to address mesh dependency". International Journal for Numerical Methods in Engineering 59.1, pp. 1–24. DOI: 10.1002/nme.857. eprint: https://onlinelibrary.wiley.com/doi/pdf/10.1002/nme.857